Environmental Science & Technology

Contaminants in Aquatic and Terrestrial Environments

Photochemical Transformations of Carbon Dots in Aqueous Environments

Benjamin P. Frank, Leslie Sigmon, Alyssa Deline, Ronald S. Lankone, Miranda Gallagher, Bo Zhi, Christy L. Haynes, and D. Howard Fairbrother

Environ. Sci. Technol., **Just Accepted Manuscript** • DOI: 10.1021/acs.est.9b07437 • Publication Date (Web): 12 Mar 2020

Just Accepted

is published by the American Chemical Society. 1155 Sixteenth Street N.W., Washington, DC 20036

Photochemical Transformations of Carbon Dots in Aqueous Environments

Benjamin P. Frank[1], Leslie R. Sigmon[1], Alyssa R. Deline[1], Ronald S. Lankone[1], Miranda J. Gallagher[1], Bo Zhi[2], Christy Haynes[2], David Howard Fairbrother[1*]

[1]Department of Chemistry, Johns Hopkins University, 3400 North Charles Street, Baltimore, Maryland 21218, United States

[2]Department of Chemistry, University of Minnesota, 207 Pleasant Street SE, Minneapolis, Minnesota 55455, United States

*Corresponding Author: D. Howard Fairbrother, Department of Chemistry, Johns Hopkins University, 3400 North Charles Street, Baltimore, Maryland 21218, United States

Email: howardf@jhu.edu

Abstract

The unique physicochemical and luminescent properties of carbon dots (CDs) have motivated research efforts towards their incorporation into commercial products. Increased use of CDs will inevitably lead to their release into the environment where their fate and persistence will be influenced by photochemical transformations, the nature of which is poorly understood. This knowledge gap motivated the present investigation of the effects of direct and indirect photolysis on citric and malic acid-based CDs. Our results indicate that natural sunlight will rapidly and non-destructively photobleach CDs into optically inactive carbon nanoparticles. We demonstrate that after photobleaching, $^{\bullet}OH$ exposure degrades CDs in a two-step process that will span several decades in natural waters. The first step, occurring over several years of $^{\bullet}OH$ exposure, involves depolymerization of the CD structure, characterized by volatilization of over 60% of nascent carbon atoms and the oxidation of nitrogen atoms into nitro groups. This is followed by a slower oxidation of residual carbon atoms first into carboxylic acids and then volatile carbon species, while nitrogen atoms are oxidized into nitrate ions. Considered alongside related CD studies, our findings suggest that the environmental behavior of CDs will be strongly influenced by the molecular precursors used in their synthesis.

Introduction

Carbon dots (CDs) are an emerging class of colloidally stable carbon-based nanomaterials with high fluorescence quantum yields and tunable emission properties.[1] As an environmentally benign alternative to inorganic quantum dots that contain toxic metals, CDs have attracted great interest for their potential in sensing,[2-3] fuel cells,[4-5] drug delivery,[6-7] and bioimaging.[8-9] As a result, the quantity of CDs entering aquatic environments will inevitably increase during the production, use, and disposal of CD-enabled products. While CDs are of similar size to other carbon-based nanomaterials such as fullerenes, they are likely to exhibit different environmental behavior due to the high surface charge imparted by the functional groups (e.g., carboxylic acid, amine, and amide groups) embedded within their structure.[10]

To date, research on the environmental behavior of CDs has largely focused on their colloidal stability,[11-14] transport,[15] and toxicity[16-17] in environmental media. Bayati et al. investigated the effect of ionic strength, pH, and natural organic matter (NOM) on the aggregation of glycerol-based CDs and aminated CDs, finding both species largely stable at the upper bound of environmental ionic strength (i.e., 10 mmol/L NaCl and $CaCl_2$) and across a pH range of 3-11.[12] Li et al. showed that graphene CDs were colloidally stable in solutions of NaCl, KCl, and $MgCl_2$ with an ionic strength of >1000 mM, but were prone to aggregation in solutions containing 1 mM $CaCl_2$.[13] Liu et al. determined that hydrothermally synthesized sodium citrate-based CDs were stable to homoaggregation in environmentally relevant pH and ionic strength conditions, but this stability could be perturbed by low pH (pH < 3) and high ionic strength conditions (> 30 mM NaCl).[11] The high degree of colloidal stability exhibited by CDs translates into high transport capacity, as exhibited by Kamrani et al., in which citric acid-based CDs readily eluted through quartz media at environmentally relevant conditions and were only partially retained in the column

even at extremely high ionic strength and low pH.[15] As a result of their colloidal stability and transport properties, CDs are likely to be present in the water column for significant periods of time. Consequently, their interactions with sunlight are likely to play an important role in determining their fate and persistence in aquatic environments.

The primary photolytic processes acting on CDs in the environment will be direct irradiation by natural sunlight and indirect photolysis via exposure to reactive oxygen species (ROS) of which hydroxyl radicals (•OH) produced by the interaction of sunlight with naturally occurring species (e.g., natural organic matter (NOM) or nitrate/nitrite)[18-20] are typically the most reactive, and as such are often used experimentally to simulate the indirect photolysis of environmental contaminants.[21-25] While the effects of direct and indirect photolysis on other carbon nanomaterials (e.g., CNTs,[26-27] GO,[24, 28] fullerenes[29-30]) have been the subject of significant research, the unique chemical and fluorescent properties of CDs are likely to impart different photochemical behavior. A recent study by Chen et al. identified that CDs synthesized via a hydrothermal route using citric acid and urea rapidly degraded into low molecular weight compounds and could be mineralized to carbon dioxide under both UVB irradiation and natural sunlight exposure.[31] These transformations occurred over the course of 2 h UVB or 8 h natural sunlight exposure and were attributed to processes involving ROS formed by the irradiation of the CDs themselves, with •OH being the dominant radical species. The rapid photodegradation and mineralization of these CDs suggest they will not persist once they are released into the environment. However, these results cannot necessarily be generalized to all CDs, as an enormous array of precursors and methods (e.g. hydrothermal, isolation from organic waste, thermal decomposition, microwave)[2-3] are currently being used in their synthesis, the effect of which on the chemical, physical, and photochemical properties of CDs remains unknown.

CDs produced from small organic acid molecules, via microwave irradiation, are some of the most widely studied for consumer and research applications due to the low cost and ease of "bottom-up" synthesis.[32] Therefore it is important to develop a mechanistic understanding of their behavior in aquatic environments. In this study, the effects of direct and indirect photolysis on microwave synthesized citric acid-based CDs (CACDs) and malic acid-based CDs (MACDs) were investigated. CDs were exposed to natural sunlight for up to 6 weeks, while the effects of indirect photolysis were simulated by exposing CD solutions to $^{\bullet}OH$ radicals generated by the photolysis of H_2O_2 under UV light. Total carbon analysis (TC), total nitrogen analysis (TN), and ion chromatography (IC) were used to identify the changes in carbon content, nitrogen content, and nitrogen speciation over time. Changes to optical properties were examined using photoluminescence (PL) spectroscopy. The physicochemical transformations of CDs were characterized by a combination of attenuated total reflectance Fourier transform infrared spectroscopy (ATR-FTIR), ^{1}H- and ^{13}C-nuclear magnetic resonance spectroscopy (NMR), and X-ray photoelectron spectroscopy (XPS). Using this suite of analytical techniques, we have identified both the photochemical transformations and the kinetics of such transformations that these CDs will undergo upon release into natural waters.

Materials and Methods

Additional details of synthetic procedures, characterization methods, photochemical exposures, and $^{\bullet}OH$ radical quantification are included in the SI. For all suspensions prepared, the initial concentration of CDs was first determined via the recorded mass of dry CD powder added to a known volume of water.

Materials

All chemicals were purchased from Sigma-Aldrich and used without further purification. Milli-Q® water (18.2 Ω, Millipore, USA) was used to prepare all aqueous solutions.

Synthesis of CDs

CDs were prepared using a bottom-up microwave-assisted pyrolysis method as described by Zhi et al.[33] Two types of CDs were synthesized, using ethylene diamine (EDA) and either citric or malic acid as precursors to form CACDs and MACDs, respectively.

Characterization of CDs

CDs were characterized initially and after exposure to the effects of direct and indirect photolysis using a combination of TC, TN, IC, ATR-FTIR, XPS, ^{1}H- and ^{13}C-NMR, and PL. Transmission electron microscopy (TEM) and UV-Vis spectroscopy were used to further characterize the as-synthesized CDs.

Exposure to Natural Sunlight

Solar irradiation experiments were conducted by adding suspensions of CDs in Milli-Q water to borosilicate glass test-tubes (16 mm outer diameter x 125 mm, Corning, USA). Sample test-tubes were sealed with PTFE-lined caps, and placed outside on a rooftop in Baltimore, MD (39° 19’ W, 76° 37’ N). Equivalent dark controls were prepared by wrapping glass test-tubes in aluminum foil, and CD-free controls were prepared identically without CDs. At time points ranging from 0 to 6 weeks, samples and controls were retrieved sacrificially for analysis. Unless otherwise specified, natural sunlight exposures were performed under ambient conditions with no sparging of the samples. Therefore, dissolved oxygen levels should be representative of those encountered in natural waters.

Exposure to ˙OH Radicals

Suspensions of MACDs and CACDs were prepared and added to quartz test tubes, sealed with an aluminum foil cap, and vented via a syringe tip. Samples were exposed to ˙OH radicals generated by the photolysis of H_2O_2 in a photochemical reactor equipped with 16 low pressure mercury lamps emitting 300 nm light (RPR 100, Southern New England Ultraviolet Company, Branford, CT, approx. 1.5×10^{17} photons/s). ˙OH exposure studies performed for TC, TN, ATR-FTIR, and XPS were all carried out at concentrations at or below 350 mg/L CD. ^{13}C-NMR experiments required a higher CD concentration (1.7×10^{4} mg/L) to achieve reasonable signal-to-noise ratio.

Determination of ˙OH Radical Dose

The total dose of ˙OH generated by the photodegradation of H_2O_2 as well as the equivalent environmental exposure time in natural surface waters (Table S1) were determined using methods described by Lankone et al.[34] Briefly, the steady-state ˙OH concentration in solution generated during the photolysis of H_2O_2 was determined via monitoring the rate of salicylic acid (i.e., a probe molecule) decomposition from an initial concentration of 0.07 mM. With this methodology, the steady-state concentration of ˙OH with CDs present in solution could be determined with a standard error of less than 10%. Duration of ˙OH exposure was also recorded, enabling a molar*time ˙OH dose to be determined. This dose (M*min) was then related to an equivalent duration of exposure to ˙OH in the natural environment, wherein the steady-state concentration ranges between 10^{-15}-10^{-17} M. [19, 24, 35] For example, a ˙OH concentration of 10^{-15} M, results in a monthly ˙OH dose of 10^{-15} M * 2.2×10^{4} min/month = 2.2×10^{-11} $\frac{M*min}{month}$. Importantly, control studies found that CD concentrations used in this study (≤ 319 mg/L) had no effect on the steady-state ˙OH concentration (Figure S1).

CD Settling Tests

Suspensions of CACDs (15 mg/L) were allowed to settle for 1 week in either MilliQ water or a mixture of NaCl, KCl, and $CaCl_2$ (4 mM Ca^{+2}, 13 mM Cl^-, 0.3 mM Na^+, 5 mM K^+) at pH 7 or 8. Supernatant was analyzed for suspended CDs using PL.

Results and Discussion

Initial CD Characterization

The as-synthesized CACDs were characterized by an emission peak at 480 nm and an absorbance below 400 nm, with a peak centered at 350 nm (Figure S2a). As-synthesized MACDs emitted most strongly at 470 nm with a broad absorbance below 400 nm and a weak peak around 350 nm (Figure S2b). TEM images (Figure S2c and S2d) of the as-synthesized CACDs and MACDs reveal spherical nanoparticles with sub-10 nm diameters. ATR-FTIR of CACDs and MACDs (Figure S3a and S3b) both exhibited broad IR features at 3280 cm^{-1}, 3085 cm^{-1}, and 2927 cm^{-1} corresponding to N-H, O-H, and C-H stretching modes, respectively.[36-37] For CACDs, features at 1700 cm^{-1} (carboxyl) and 1646 cm^{-1} (amide) are attributed to carbonyl (C=O) stretches,[38-39] while the feature at 1547 cm^{-1} is indicative of an N-H bend in an amide group (O=C-NH);[37, 40] MACDs share the same carbonyl bands, however the N-H bend occurs at 1527 cm^{-1}.[37, 40-41] The C (1s) envelope of the native CDs, as measured by XPS, contained contributions from C-C and C-H species centered at 285 eV, with a higher binding energy shoulder at ~ 288 eV due to the presence of more oxidized carbon atoms (e.g. amide and carboxyl groups; Figure S4 and S5). It should be noted that due to their small size (i.e., diameters < 10 nm), XPS spectra reflect the entire CD nanoparticle with respect to composition and chemical bonding environment.

Effects of Direct Photolysis

Upon entering aquatic environments, CDs will immediately experience the effects of direct photolysis due to their absorbance within the solar power distribution reaching the earth's surface (Figure S6a). Photoluminescence (PL) spectroscopy was used to monitor the fluorescent properties of CDs after exposure to sunlight and artificial indoor light, while changes in composition and chemical bonding were evaluated using a combination of TC/TN, XPS, ATR-FTIR, and ^{1}H-NMR.

CACDs exposed to natural sunlight experienced rapid photobleaching, as their fluorescence disappeared after 12 h of irradiation, observed both spectroscopically (Figure 1a, S7) and visually (Figure S8). This low photostability is in stark contrast to the persistence of fluorescence (Figure S9a) observed under artificial laboratory lighting. This difference in photostability is attributed to the differences in overlap between the absorbance spectrum of the CDs and the respective emission spectra from natural sunlight (solar irradiance, Figure S6a) and fluorescent bulbs (Figure S9b). Thus, it is likely that the < 400 nm component of natural sunlight drives photobleaching of CDs in the environment. The loss of fluorescence induced by exposure to sunlight was also found to be more rapid in solutions initially saturated with O_2, but unaffected in solutions sparged with N_2 (Figure 1b). This behavior indicates that photobleaching in natural sunlight likely involves reactions with ROS formed via the presence of dissolved oxygen in solution.

Despite the rapid loss of fluorescence in CD solutions (i.e., < 12 h), exposure of up to 6 weeks of sunlight had no observable effect on the carbon or nitrogen content as exhibited by TC and TN (Figure 1c). Similarly, XPS data revealed that the composition within the CACDs (Figure 2a) and MACDs (Figure S10) as well as the chemical bonding environment within both CACDs (Figures 2b, S4) and MACDs (Figures S5) also remained constant over the course of the 6-week

exposure. ATR-FTIR spectra of CACDs and MACDs (Figure 2c) were largely unchanged after 6 weeks of exposure to sunlight, though for CACDs, loss of intensity at 1547 cm^{-1} was observed during the first two weeks of outdoor exposure, suggesting photobleaching could be driven through proton abstraction from the amide groups initially present in the CD structure, though not extensively enough to meaningfully change the CD composition.

^{1}H-NMR spectra of CACDs acquired before and after photobleaching also indicated only minor chemical changes to proton bonding environments (Figure 2d). As-synthesized CACDs featured clusters of ^{1}H-NMR peaks in several diagnostic regions: 1.8 ppm to 2.5 ppm, 2.5 ppm to 4.5 ppm, and at 8.4 ppm, indicative of protons in the α- or β-position to carbonyl or amide groups,[42-44] protons bound to or in the α-position to oxidized carbon species (i.e., alcohol, ether, ester, carbonyl),[42, 45] and non-exchangeable amide protons[46-48] respectively. In contrast, no carboxylic acid protons were observed due to exchange of these acidic protons in the (D_2O) solvent. The photobleached CACDs exhibited a largely similar ^{1}H-NMR spectrum to the parent CACDs. The only changes observed were the loss of peak intensity at 4.2 ppm and the increase in intensity of the peak at 8.4 ppm, likely indicating some degradation of the amide groups initially present in the CDs.

Collectively, these findings indicate that the principle effect of natural sunlight on organic acid-based CDs immediately after entering an aquatic environment is rapid (i.e., < 12 h) photobleaching (Figure 1a) in a process modulated by the relative level of dissolved oxygen therein (Figure 1b). While the initial rate of photobleaching may vary to some degree dependent on the concentration of dissolved oxygen available to generate ROS, the complete photobleaching of CDs is expected to occur in all aqueous environments, irrespective of dissolved oxygen content (Figure 1b). Findings also indicate that the CD structure and composition will remain largely unchanged

during photobleaching, supported by mass-recovery studies which demonstrated that 101.4 % +/- 2.1 % of CD mass is recovered after 21 d of natural sunlight exposure (see SI for details).

Interestingly, these findings contrast with a study published by Chen et al., in which it was reported that citric acid/urea CDs were rapidly volatilized in totality after 8 h of natural sunlight exposure due to extensive structural decomposition driven by CD-produced $^{\bullet}OH$.[31] We posit one possibility for the contrasting photochemical behavior observed between these studies is that the different structural features present in the two different types of CDs, arising by virtue of the different precursors used (e.g., urea features a carbonyl group which EDA lacks), strongly regulate the persistence of CD photoactivity, the overall phototransformation pathway, and resultant kinetics of sunlight driven degradation. While we did not observe degradation or volatilization for CDs exposed to sunlight in the present study, the photobleaching and comparatively small changes that did occur to the CDs indeed could arise from similar reactions between CD-generated ROS and the CDs themselves[31] (e.g., $^{\bullet}OH$-driven proton abstraction)[49] as suggested by the increase in photobleaching rate with increased dissolved oxygen content.

Importantly, because as-synthesized CDs remained colloidally stable in the presence of divalent cations known to destabilize other nanomaterials (Figure S11), the lack of significant changes to the physicochemical properties of CDs after photobleaching suggests that they will remain colloidally stable in natural environments after irradiation by natural sunlight. Specifically, spectroscopic measurements (i.e., XPS, ATR-FTIR) of the photobleached CDs indicate the retention of negatively charged oxygen-containing functional groups (i.e., carboxyl, hydroxyl) which are responsible for the electrostatic repulsion between CDs, an effect which is responsible for the colloidal stability of carbon dots[50-54] as well as other carbon nanomaterials (CNTs,[55-57] graphene[58-60]) in aqueous environments. Consequently, photobleached CDs can be expected to

remain stable for long periods in the water column where they will be subject to reactions with ROS (primarily •OH) generated by the irradiation of common constituents of natural water (NOM, NO_3^-).[18-20]

Effects of Indirect Photolysis.

To assess the effects of indirect photolysis on CDs, CACD and MACD suspensions were exposed to •OH produced via 300 nm irradiation of H_2O_2. 300 nm irradiation of CDs in the absence of H_2O_2 photobleached CDs without any measurable structural changes. A previous analytical study enabled us to determine the Molar × time dose of •OH generated during H_2O_2 photolysis (Table S1), permitting comparison to the equivalent dose of •OH CDs would experience in the natural environment. The kinetics of CD photodegradation by •OH was assessed using TC and TN, while reaction products were identified through a combination of IC, ATR-FTIR, ^{13}C-NMR, and XPS.

TC data indicated that during •OH exposure, both CACDs and MACDs reacted in two well defined temporal stages. First, ~ 60% of carbon atoms initially present in both CD types were lost after a 1.4×10^{-9} M*min exposure to •OH (Figure 3a). Following this rapid and extensive loss of carbon atoms, the residual carbon-containing species were significantly less susceptible to further •OH-mediated degradation during the second stage of the reaction as the •OH dose increased beyond 1.4×10^{-9} M*min •OH. At an •OH dose of 2.8×10^{-8} M*min, the carbon content only decreased by an additional 10% for MACDs, while a dose of 4.0×10^{-8} M*min •OH only decreased the carbon content by 15% for CACDs.

Complementary TN analysis (Figure 3b) revealed that the total nitrogen content was relatively insensitive to •OH exposure (•OH doses of 4.0×10^{-8} M*min), in marked contrast to the

considerable loss of carbon (compare Figures 3a and 3b). Although the total nitrogen content remained essentially constant during •OH exposure, nitrogen speciation evolved. Specifically, the production of nitrate was observed for •OH doses in excess of 5.5×10^{-9} M*min (Figure 3b) and increased steadily until all CD nitrogen atoms were converted into nitrate ions. The constant TN content coupled with the steady increase in nitrate concentration in solution indicates that over time the •OH-driven degradation of CDs will produce nitrate ions.

ATR-FTIR spectra shown in Figure 4a provide spectroscopic evidence of two distinct phases in the reaction of MACDs with •OH. The first phase of degradation was initiated upon exposure to an •OH dose of 6.9×10^{-10} M*min, which resulted in a decrease in intensity of the amide N-H bending mode at 1527 cm^{-1}, and a red-shift of the (carboxylic) C=O stretch to 1680 cm^{-1} indicative of a change in the chemical bonding environment in the MACDs. The simultaneous diminishment and transformation of these features indicates that •OH-mediated decomposition of CDs involves a cleavage of the amide moieties initially present in the CD backbone. After •OH exposure increased from 6.9×10^{-10} M*min to 1.4×10^{-9} M*min, the amide groups initially present in the CDs had been oxidized into nitro groups(i.e., NO_2), as evidenced by the simultaneous loss of the O=C-NH bend at 1527 cm^{-1} and the appearance of the ν_4/ν_1 stretches of nitro groups at 1590 cm^{-1} and 1414 cm^{-1}, respectively.[61] Additionally, the appearance of peaks at ~ 3400 cm^{-1} and 1100 cm^{-1} indicate the formation of hydroxyl groups in the photoproducts[38, 62] whose sharpness and peak positions are very similar to the hydroxyl features present in malic acid (Figure 4b). By a •OH dose of 1.4×10^{-9} M*min, the previous carbonyl feature at 1700 cm^{-1} had shifted and is now centered on 1680 cm^{-1} , indicating that the carbonyl species are now in a more highly hydrogen-bound chemical environment (i.e., small carboxylic acids, such as malic acid). As the •OH dose increases, new bands at 1313 cm^{-1}/831 cm^{-1} also emerge which can be assigned to and the ν_3 stretch

272 (E')/ν_2 bend (A_2'') of nitrate ions.[63] Collectively, the formation of these oxidized nitrogen groups
273 and the similarity of degraded CD spectra to malic acid strongly suggests that CDs were
274 depolymerized in the presence of •OH through the cleavage of their initial amide bonds to form
275 nitro groups and malic acid photofragments.

276 The second phase of degradation shown by ATR-FTIR was observed for •OH doses beyond
277 1.4×10^{-9} M*min, and is defined as being the period of exposure during which the spectra remained
278 relatively unchanged with increasing •OH dose, aside from an increase in nitrate and nitro peak
279 intensities. ATR-FTIR spectra observed for the solid phase (i.e., lyophilized) species produced by
280 MACDs exposed to •OH doses in excess of 5.5×10^{-9} M*min continued to exhibit peaks similar to
281 those of sodium nitrate and the solid malic acid precursor (Figure 4b, common peaks: free O-H at
282 3400 cm^{-1}, carboxy C=O at 1680 cm^{-1}, and O-H deformation at 1100 cm^{-1}). Furthermore, Figure
283 4b demonstrates sustained exposure of both MACDs and CACDs to •OH in excess of 5.5×10^{-10}
284 M*min resulted in the formation of near identical photoproducts as suggested by the similarity of
285 their spectra. It should be noted that XPS and ATR-FTIR analysis was not possible for •OH doses
286 above 1.1×10^{-8} M*min, as the mass loss due to volatilization of carbon (as shown by TC) precluded
287 sufficient sample recovery.

288 XPS spectra of CACDs exposed to •OH also indicate a two-phase degradation process.
289 During the first period of degradation, •OH exposure up to 1.4×10^{-9} M*min •OH resulted in a loss
290 of higher binding energy features (i.e., carbonyl carbon), and the C (1s) region was dominated by
291 the C-C/C-H species at 285 eV with only a small shoulder at 288 eV (Figure 5a). The CDs then
292 entered the second phase of •OH exposure from doses of 5.5×10^{-9} M*min to $1.1*10^{-8}$ M*min, at
293 which point the carbonyl feature reemerged in the C (1s) region at 288 eV. XPS analysis also
294 revealed that exposure to •OH produced an overall decrease in the carbon content and a small

295 increase in the nitrogen content of the non-volatile photoproducts (Figure S12). Specifically,
296 CACDs were initially composed of 55% carbon and 15% nitrogen, but exposure to $1.1*10^{-8}$
297 M*min •OH led to products that contained 35% carbon and 20% nitrogen. This enrichment of
298 nitrogen with increasing •OH exposure as measured by XPS is qualitatively consistent with the
299 trends observed by TC/TN in that it further indicates that carbon was lost and volatilized from the
300 CDs, while nitrogen atoms remain associated with the CD photoproduct.

301 The ^{13}C-NMR of CACDs exposed to •OH also indicated extensive degradation to the CDs.
302 Photobleached CACDs (Figure 5b) prior to •OH exposure contained various carbon functional
303 groups including carboxylic acids/amides (160-180 ppm)[64], alcohols/ethers (70-90 ppm),[65-66] and
304 both substituted (i.e., branched) and primary alkane carbons centered around 30-50 ppm and 10-
305 30 ppm, respectively.[67-68] After a •OH dose sufficient to cause a loss of 60% TC, ^{13}C-NMR was
306 performed again to assess the CDs nearing the end of the first phase of degradation (see Figure 3).
307 The resultant ^{13}C-NMR indicates that the CDs degraded through the loss of substituted/branched
308 alkane groups (30 ppm to 50 ppm). This suggests that the crosslinked network initially present in
309 the CDs was degraded during •OH exposure. Interestingly, the growth of one peak around 165
310 ppm, likely a carboxyl species, agrees with the increase in such species as shown with ATR-FTIR
311 and XPS spectra.

312 To contextualize these results in terms of the equivalent environmental •OH exposure, we
313 applied a methodology developed by Lankone et al. which allowed the integrated •OH dose to be
314 benchmarked to the maximum •OH dose a sample would experience during one month of exposure
315 in sunlit waters (10^{-15} M * 2.2×10^{4} min/month = 2.2×10^{-11} $\frac{M*min}{month}$). For example, exposure to a
316 solution of H_2O_2 at an initial concentration of 100 mM, as it is photolyzed for 4 hours results in
317 CD exposure of 1.4×10^{-9} M*min; this dose corresponds to an equivalent environmental exposure

of approximately 64 months ($\frac{1.4*10^{-9}M*min}{2.2*10^{-11}\frac{M*min}{month}}$). In this study, relations to environmental timescale were done under the assumption that CDs consistently experience the maximum •OH dose (i.e., 10^{-15} M) in the environment, though calculations based on the full range of $[^{\bullet}OH]_{ss}$ are reported in the SI (Table S1). Using these calculations and assuming an environmental steady state •OH concentration of 10^{-15} M, we can discuss CD photodegradation by indirect photolysis in terms of the equivalent environmental timescale.

The two-step degradation process first observed with TC and TN data (Figure 3a and 3b) can now be interpreted to indicate that the period of initial CD degradation in the presence of •OH occurs over approximately 64 +/- 5 months of indirect photolysis in sunlit waters. During this time, as indicated by ATR-FTIR and XPS, the CDs are depolymerized via the cleavage of amide groups, resulting in the formation of nitro groups and carboxylic acid species. Additionally, TC indicates that 60% of carbon atoms are lost from solution, most likely as volatile species, similar to the reactions of •OH with GO which evolve CO_2 as an end product.[24] We note the rate of loss of the amide feature at 1527 cm^{-1} closely corresponds to the rate at which the initial carbon volatilization occurs (compare TC and ATR-FTIR data in Figures 3a and 4a, respectively), suggesting that the first step in the degradation of CDs by •OH is hydrogen abstraction from N-H and/or C-H groups,[49, 69-70] leading to the degradation of amide linkages. Additional evidence of this depolymerization is seen in ^{13}C-NMR data via the loss of C=C (120 ppm) and substituted/branched alkane character (30-50 ppm), representing the degradation of crosslinked character within the CDs, resulting in the primary alkane signature which persists in the resultant photoproducts (10-30 ppm) which are also carboxylated as seen in both ATR-FTIR (1680 cm^{-1}; Figure 4a) and ^{13}C-NMR (165 ppm; Figure 5b). The redshift of the carboxyl C=O stretch coupled with the persistence of primary alkanes seen in ^{13}C-NMR provides evidence for the evolution of low molecular weight carboxylic acids after

depolymerization which are less sterically hindered than in the parent CD, thus able to participate in more extensive hydrogen bonding.[38]

In contrast to the significant loss/volatilization of carbon atoms, the TN and ATR-FTIR data reveal that during the first 64 +/- 5 months of environmental exposure, there is little to no change in the total nitrogen content, although the nitrogen species initially present in the CDs have been converted/oxidized into nitro groups by $^{\bullet}$OH. This oxidation occurs over the same $^{\bullet}$OH dose as the loss in amide character in ATR-FTIR (1646 cm^{-1}), suggesting that nitrogen atoms involved in amide linkages in the parent CDs are oxidized into nitro groups after cleavage during indirect photolysis.

Following the initial $^{\bullet}$OH-mediated depolymerization of the CD structure, the second phase of indirect photolysis is observed for cumulative $^{\bullet}$OH doses in excess of approximately $1.4*10^{-9}$ M*min, or beyond the first 64 +/- 5 months of environmental exposure, and is characterized by a much slower decrease in carbon content. During this phase, residual carbon atoms are further oxidized by $^{\bullet}$OH, leading to a significant increase in the concentration of highly oxidized photoproducts structurally similar to the dicarboxylic acids used in the original CD synthesis (e.g. malic acid as shown with ATR-FTIR in Figure 4b), and related carboxylic acids (e.g. glutaric acid, Figure S13). The formation of carboxylated carbon species is consistent with the increase in concentration of the C(1s) shoulder above 286 eV in XPS. Because both CACDs and MACDs generated photoproducts with similar spectroscopic signatures, this degradation pathway is likely generalizable to CDs synthesized from EDA and carboxylic acid precursors.

When the changes in composition and structure are considered together, our results indicate that during this second stage of indirect photolysis, residual carbon atoms are oxidized by $^{\bullet}$OH to carboxyl groups which then serve as precursors for the formation of volatile species[70] such as

364 CO_2[24] or acetone.[71] Continued •OH-mediated oxidation of previously formed nitro groups leads to
365 the evolution of nitrate ions[72] as indicated by the IC and ATR-FTIR data (Figures 3b and 4a). Thus,
366 extrapolation of these trends to sustained (maximum) •OH exposure in the natural environment, in
367 excess of the 43 years of equivalent exposure simulated in laboratory studies, indicates CDs would
368 eventually degrade such that all carbon atoms will be volatilized while nitrogen atoms are
369 stoichiometrically converted into nitrate ions.

370 The reason for the two distinct temporal regimes of carbon loss, however, remains
371 somewhat unclear. One possible explanation is that the more recalcitrant carbon atoms seen in the
372 second phase of the process are associated with fragments containing carbon-nitrogen bonds
373 residual from reactions of •OH with the parent CDs. This interpretation is supported by IC data
374 which clearly shows that the formation of nitrate ions from the CDs requires a dose of •OH in
375 excess of 5.5×10^{-9} M*min. The evolution of nitrate ions from nitro groups requires C-N bond
376 cleavage, a limiting prerequisite step in the volatilization of these carbon atoms compared to those
377 in other bonding environments.

378

379 **Environmental Implications**

380 Due to their highly charged surface and small size, CDs are colloidally stable in the water
381 column.[11-14] Thus, the effects of both direct and indirect photolysis will play an important role in
382 determining the fate and persistence of CDs in aquatic environments. In contrast to their
383 photostability under illumination in laboratory settings (i.e., under fluorescent lighting), the citric
384 and malic acid-based CDs investigated in this study will rapidly photobleach after only a few hours
385 of direct photolysis by natural sunlight, likely precluding the use of these particular CDs as sensors
386 in outdoor settings. Once the CACDs and MACDs have photobleached, the resultant carbon

nanoparticles exhibit similar physicochemical properties to the parent CDs, suggesting a high degree of colloidal stability. Consequently, these photobleached CDs will persist for extended periods of time in the environment while being difficult to monitor or track due their poor light scattering properties and lack of fluorescent signature.

Ultimately, photobleached CDs will be degraded by indirect photolysis via reactions with ROS, primarily $^{\bullet}OH$ produced by exposure of NOM and other constituents of water (e.g., metal ions, nitrate, dissolved oxygen) to natural sunlight.[20] Based on the relation to environmental timescale which was used (assuming exposure to the maximum environmental $[^{\bullet}OH]_{ss}$),[34] the first stage of this indirect photolysis will occur over the course of approximately 5-6 years of environmental exposure in sunlit waters, resulting in depolymerization of the CD via cleavage of its amide bonds and the oxidation of a majority of the carbon atoms in the CDs into volatile carbon species (e.g., CO_2 and acetone). Over the same time span, nitrogen atoms will be oxidized into nitro groups bound to fragments of the parent CDs. Environmental exposure of the residual photoproducts will lead to the formation of carboxylic acid species similar to the organic acids used in the CD synthesis (e.g. malic acid). These carboxylic acids will serve as precursors to the production of volatile carbon species, a process which will continue until all carbon atoms in the CDs are ultimately mineralized (timespan of several decades based on TC trend). In contrast, nitrogen atoms in the CDs will be stoichiometrically oxidized from nitro groups into nitrate ions as indicated by IC data (half-life roughly 75 years). Given the projected lifetime and colloidal stability of photobleached CDs and their photoproducts throughout this prolonged photodegradation process, future studies identifying the environmental impact of these various intermediate species will be prudent.

409 A comparison of the results from this study with previous studies highlights the diversity
410 of photochemical transformations experienced by carbon-based nanomaterials in the environment.
411 For example, GO rapidly photofragments in natural sunlight as a result of the reactivity of the
412 highly strained epoxide groups that exist on its surface, leading to the formation of reduced
413 graphene oxide species (rGO) and the evolution of CO_2.[28] Conversely, oxidized carbon nanotubes
414 (CNTs) do not fragment upon exposure to sunlight or ROS, but rather undergo
415 photodecarboxylation, causing them to lose surface charge which leads to sedimentation.[26]
416 Aggregates of fullerenes are prone to ROS-driven degradation by sunlight, leading to
417 disaggregation, the formation of dissolved organic species, and eventual mineralization.[29]
418 However, under simulated sunlight[30] and UVA light conditions,[73] fullerenes showed a higher level
419 of resistance to mineralization, only exhibiting surface oxidation. These observations clearly
420 indicate that the structure and physicochemical properties of carbon nanomaterials play a
421 determinant role in regulating their photochemical reactions in the environment. With this in mind,
422 it is not unreasonable that the photochemical transformations of CDs will be sensitive to their
423 chemical structure and composition.

424 Although the phototransformations of the microwave-synthesized CACDs and MACDs
425 using ethylene diamine outlined in this study parallel one another and were structurally stable for
426 6 weeks in natural sunlight, it has been reported that CACDs synthesized via a hydrothermal route
427 using urea are completely mineralized in sunlight after less than one day at concentrations similar
428 to the ones used in the present study (50 mg/L).[31] Thus, the intrinsic chemical and physical
429 characteristics of CDs imparted via their precursors appear to dictate their photostability. As such,
430 it will be important to identify the different phototransformations of CDs synthesized with a wide
431 variety of precursors and synthetic pathways. Additionally, a detailed understanding of the

mechanisms and influential factors which dictate CD photobleaching will be needed to improve photostability if CDs are to be used as environmental sensors and tracers in outdoor settings.

Acknowledgements

This work was supported by National Science Foundation under the Center for Sustainable Nanotechnology, CHE-1503408.The CSN is part of the Centers for Chemical Innovation Program. LRS is supported by the National Science Foundation Graduate Research Fellowship Program under Grant No. DGE-1746891. The authors would like to thank Steven Chow for assistance with ion chromatography measurements, the Materials Characterization Facility at Johns Hopkins University, and the U.S. Department of Energy (DOE)/NREL/ALLIANCE for the solar irradiance data as well as Casey Smith for assistance with figures and Dylan Brach for CD photographs. TEM characterization was carried out in the Characterization Facility, University of Minnesota, which receives partial support from the MRSEC program (DMR-1420013).

Supporting Information

Detailed calculation of $^{\bullet}OH$ dose and relation to environmental timescale (Table S1, Figure S1) and experimental procedures for CD synthesis and characterization (PL, UV-Vis, TEM, ATR-FTIR, XPS, TC, TN, IC, ^{1}H- and ^{13}C-NMR; Figures S2, S3, S4, S5). CD absorption compared to solar emission spectrum (Figure S6) and emission spectrum of fluorescent bulbs (Figure S9), effects of photobleaching after exposure to natural sunlight (Figure S7, S8, S10) along with stability studies of CDs in the presence of divalent cations (Figure S11). Additional figures illustrating change in XPS composition of CDs after $^{\bullet}OH$ exposure (Figure S12) are included and ATR-FTIR comparing degraded MACDs to glutaric acid (Figure S13).

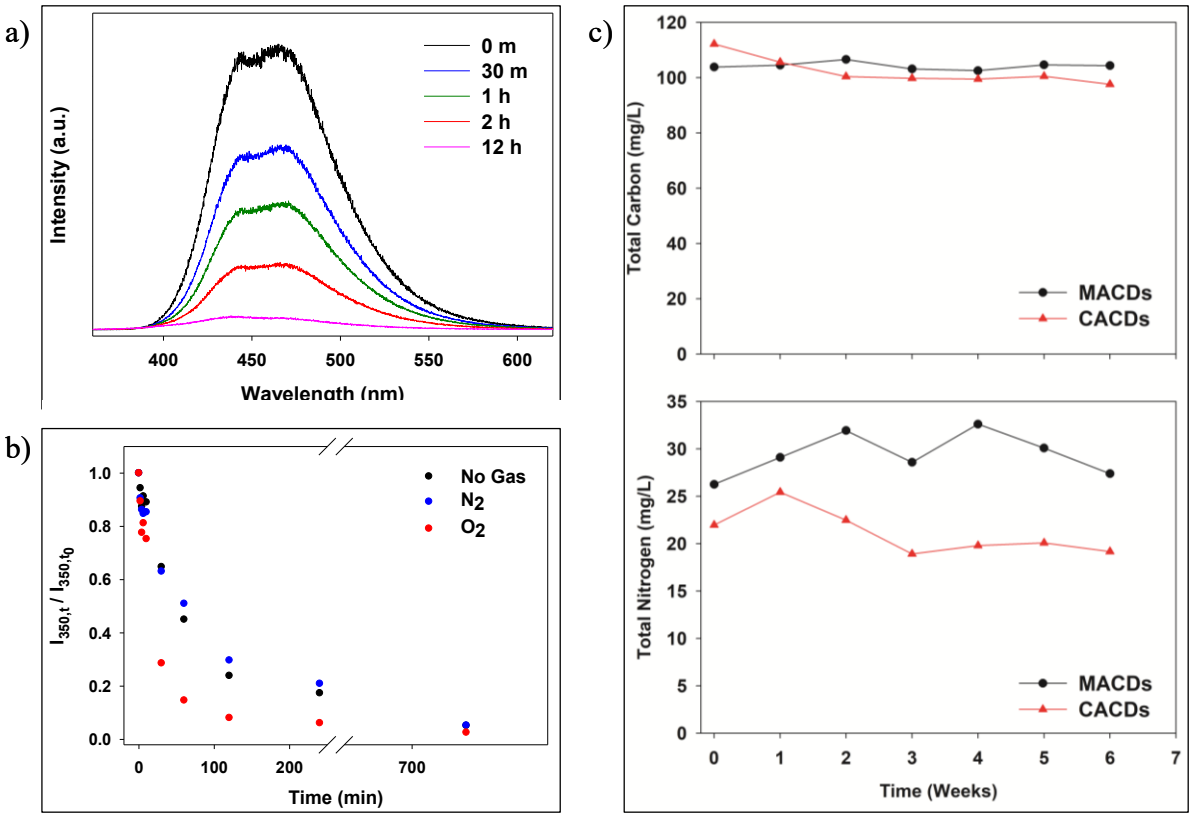

Figure 1. Effect of natural sunlight on CDs. a) Emission profiles of CACDs after exposure to 0 min (black), 30 min. (blue), 1 hr. (green), 2 hr. (red), and 12 hr. (pink) of natural sunlight. b) Emission of CACDs at 350 nm (black) compared to emission of CACDs after sparging with N_2 (blue) or O_2 (red) gas as a function of exposure to natural sunlight. c) Total carbon (top) and total nitrogen (bottom) concentration of CACDs (red triangles) and MACDs (black circles) after exposure to 0-6 weeks of natural sunlight in non-sparged water.

455

456

457

458

459

460

461

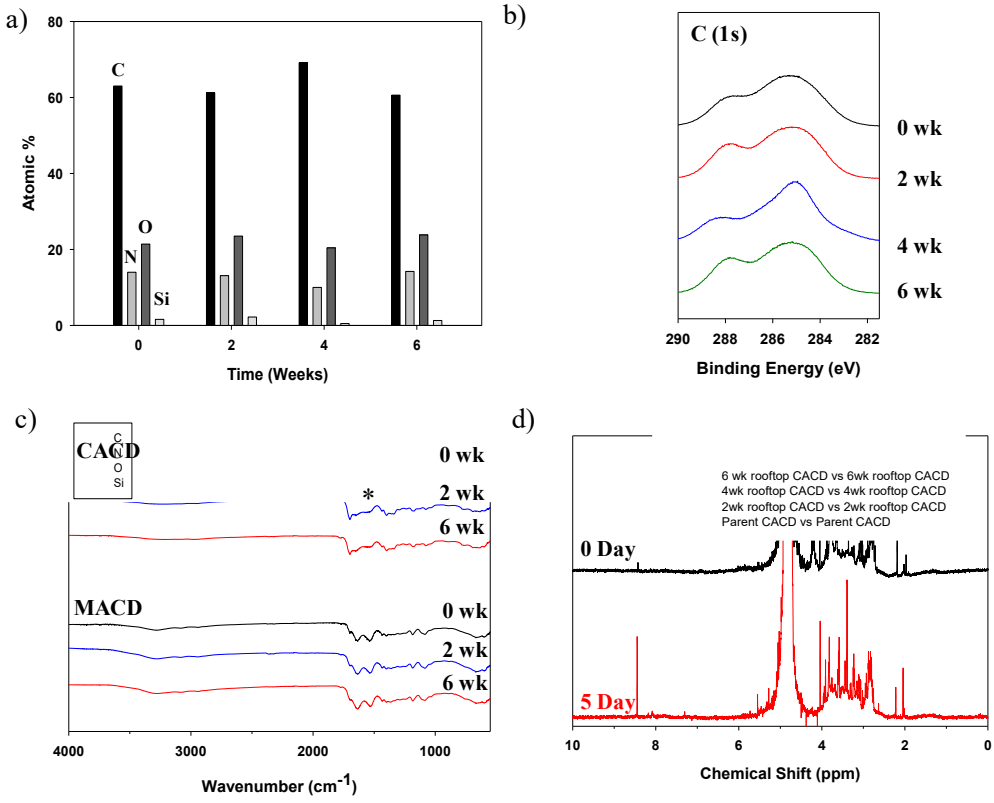

Figure 2. Effect of natural sunlight on CD structure. a) Atomic composition of lyophilized CACDs after natural sunlight exposure for 0-6 wk as determined with XPS. b) XPS C (1s) regions of lyophilized parent CACDs after 0 (black), 2 (red), 4 (blue), and 6 (green) weeks of natural sunlight exposure. (c) ATR-FTIR spectra of CACDs (top) and MACDs (bottom) exposed to natural sunlight for 0, 2, and 6 weeks, with (*) indicating the N-H bend at 1547 cm^{-1}. (d) ^{1}H-NMR spectra of CACDs (black) and CACDs exposed to 5 days of natural sunlight (red).

462

463

464

465

466

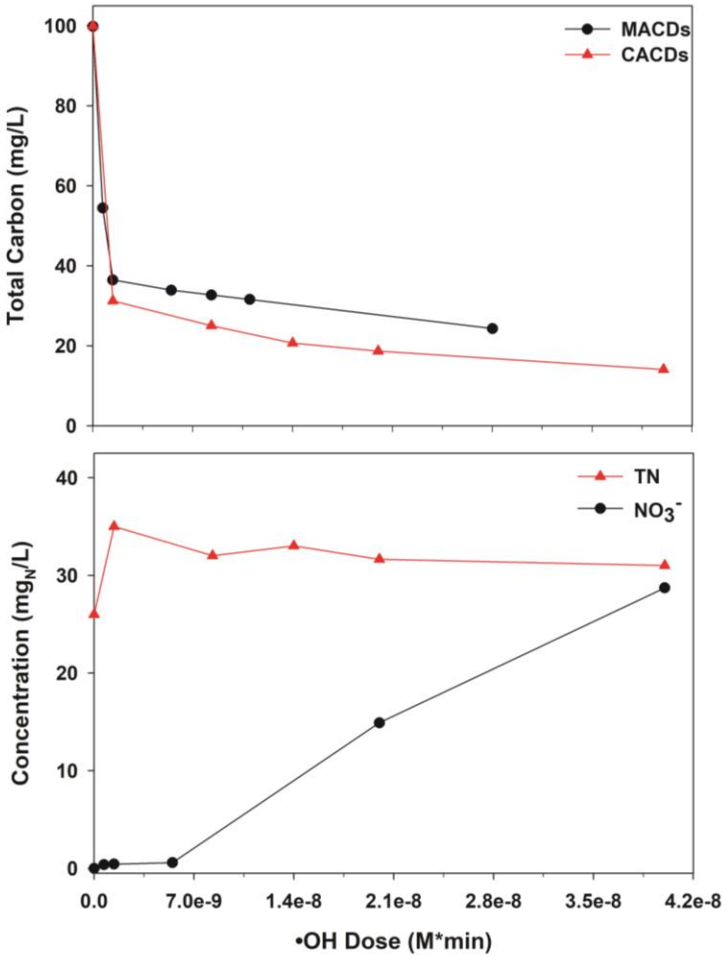

Figure 3. Degradation of CDs by ˙OH. (a) Total carbon concentration of MACD (black) and CACD (red) as a function of ˙OH dose. (b) Total nitrogen (red) and nitrate concentration (black) of CACD solution in terms of mg/L nitrogen as a function of ˙OH dose.

467

468

469

470

471

472

473

474

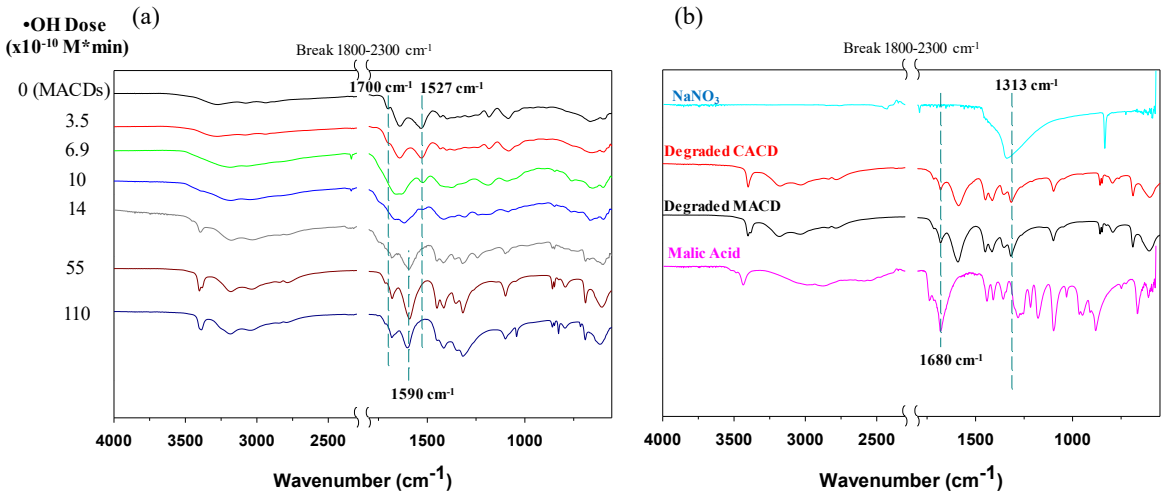

Figure 4. ATR-FTIR of lyophilized MACDs after exposure to different ˙OH doses. (a) MACDs (black) after exposure to 3.5×10^{-10} M*min (red), 6.9×10^{-10} M*min (light green), 1.0×10^{-9} M*min (blue), 1.4×10^{-9} M*min (grey), 5.5×10^{-9} M*min (dark red), and 1.1×10^{-8} M*min (dark blue) ˙OH. Insufficient masses of photoproducts were recovered for CDs reacted with ˙OH doses > 1.1×10^{-8} M*min, precluding ATR-FTIR analysis. Dotted lines mark carboxyl C=O (stretch, 1700 cm^{-1}), N-H (bend, 1527 cm^{-1}), and nitro (stretch, 1590 cm^{-1}) modes. (b) Degradation products of CACDs (red) and MACDs (black) after exposure to 5.5×10^{-9} M*min ˙OH shown in comparison to malic acid (MA, pink) and sodium nitrate (blue). Dotted lines mark carboxyl C=O (stretch, 1680 cm^{-1}) and nitrate ν_3 (stretch, 1313 cm^{-1}) modes.

475

476

477

478

479

480

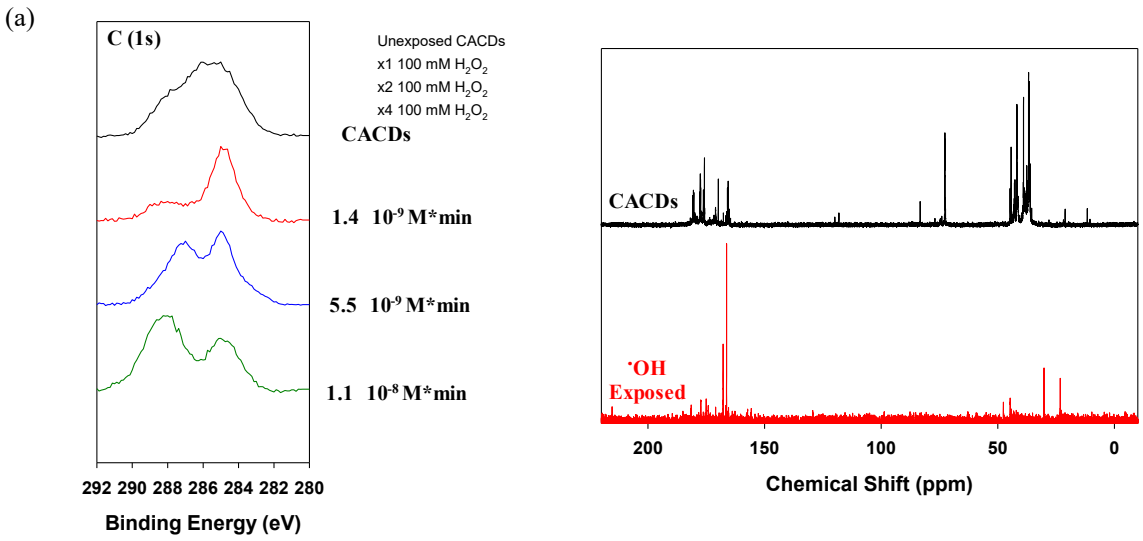

Figure 5. a) C (1s) region of lyophilized CACDs (black) after exposure to a dose of 1.4×10^{-9} M*min (red), 5.5×10^{-9} M*min (blue), and 1.1×10^{-8} M*min (green) •OH. Insufficient masses of photoproducts were recovered for CDs reacted with •OH doses > 1.1×10^{-8} M*min, precluding XPS analysis. b) ^{13}C-NMR of photobleached CACDs in D_2O before (black) and after (red) exposure to 5.7×10^{-8} M*min •OH. At the significantly higher CD concentration required for NMR (1.7×10^{4} mg/L), this •OH dose leads to the loss of 60% of carbon from solution as determined with TC.

481

482

483

References

1. Yan, F.; Sun, Z.; Zhang, H.; Sun, X.; Jiang, Y.; Bai, Z., The fluorescence mechanism of carbon dots, and methods for tuning their emission color: a review. *Microchimica Acta* **2019,** *186* (8), 583.
2. Liu, M. L.; Chen, B. B.; Li, C. M.; Huang, C. Z., Carbon dots: synthesis, formation mechanism, fluorescence origin and sensing applications. *Green Chem.* **2019,** *21* (3), 449-471.
3. Huang, S.; Li, W.; Han, P.; Zhou, X.; Cheng, J.; Wen, H.; Xue, W., Carbon quantum dots: synthesis, properties, and sensing applications as a potential clinical analytical method. *Anal. Methods* **2019,** *11* (17), 2240-2258.
4. Zhang, Z.; Zhang, J.; Chen, N.; Qu, L., Graphene quantum dots: an emerging material for energy-related applications and beyond. *Energ. Environ. Sci.* **2012,** *5* (10), 8869-8890.
5. Fei, H.; Ye, R.; Ye, G.; Gong, Y.; Peng, Z.; Fan, X.; Samuel, E. L. G.; Ajayan, P. M.; Tour, J. M., Boron- and nitrogen-doped graphene quantum dots/graphene hybrid nanoplatelets as efficient electrocatalysts for oxygen reduction. *ACS Nano* **2014,** *8* (10), 10837-10843.
6. Hettiarachchi, S. D.; Graham, R. M.; Mintz, K. J.; Zhou, Y.; Vanni, S.; Peng, Z.; Leblanc, R. M., Triple conjugated carbon dots as a nano-drug delivery model for glioblastoma brain tumors. *Nanoscale* **2019,** *11* (13), 6192-6205.
7. Zhang, Z.; Lei, Y.; Yang, X.; Shi, N.; Geng, L.; Wang, S.; Zhang, J.; Shi, S., High drug-loading system of hollow carbon dots–doxorubicin: preparation, in vitro release and pH-targeted research. *J. Mater. Chem. B* **2019,** *7* (13), 2130-2137.
8. Zhi, B.; Cui, Y.; Wang, S.; Frank, B. P.; Williams, D. N.; Brown, R. P.; Melby, E. S.; Hamers, R. J.; Rosenzweig, Z.; Fairbrother, D. H.; Orr, G.; Haynes, C. L., Malic acid carbon dots: from super-resolution live-cell imaging to highly efficient separation. *ACS Nano* **2018,** *12* (6), 5741-5752.
9. Boakye-Yiadom, K. O.; Kesse, S.; Opoku-Damoah, Y.; Filli, M. S.; Aquib, M.; Joelle, M. M. B.; Farooq, M. A.; Mavlyanova, R.; Raza, F.; Bavi, R.; Wang, B., Carbon dots: Applications in bioimaging and theranostics. *Int. J. Pharm.* **2019,** *564*, 308-317.
10. Sciortino, A.; Cannizzo, A.; Messina, F., Carbon nanodots: a review—from the current understanding of the fundamental photophysics to the full control of the optical response. *C — Journal of Carbon Research* **2018,** *4* (4), 67.
11. Liu, X.; Li, J.; Huang, Y.; Wang, X.; Zhang, X.; Wang, X., Adsorption, aggregation, and deposition behaviors of carbon dots on minerals. *Environ. Sci. Technol.* **2017,** *51* (11), 6156-6164.
12. Bayati, M.; Dai, J.; Zambrana, A.; Rees, C.; Fidalgo de Cortalezzi, M., Effect of water chemistry on the aggregation and photoluminescence behavior of carbon dots. *J. Environ. Sci.* **2018,** *65*, 223-235.
13. Li, Q.; Chen, B.; Xing, B., Aggregation kinetics and self-assembly mechanisms of graphene quantum dots in aqueous solutions: cooperative effects of pH and electrolytes. *Environ. Sci. Technol.* **2017,** *51* (3), 1364-1376.
14. Dager, A.; Uchida, T.; Maekawa, T.; Tachibana, M., Synthesis and characterization of mono-disperse carbon quantum dots from fennel seeds: photoluminescence analysis using machine learning. *Sci. Rep.* **2019,** *9* (1), 14004.
15. Kamrani, S.; Rezaei, M.; Kord, M.; Baalousha, M., Transport and retention of carbon dots (CDs) in saturated and unsaturated porous media: role of ionic strength, pH, and collector grain size. *Water Res.* **2018,** *133*, 338-347.
16. Havrdova, M.; Hola, K.; Skopalik, J.; Tomankova, K.; Petr, M.; Cepe, K.; Polakova, K.; Tucek, J.; Bourlinos, A. B.; Zboril, R., Toxicity of carbon dots – effect of surface functionalization on the cell viability, reactive oxygen species generation and cell cycle. *Carbon* **2016,** *99*, 238-248.

17. Tabish, T. A.; Scotton, C. J.; Ferguson, D. C. J.; Lin, L.; Veen, A. v. d.; Lowry, S.; Ali, M.; Jabeen, F.; Ali, M.; Winyard, P. G.; Zhang, S., Biocompatibility and toxicity of graphene quantum dots for potential application in photodynamic therapy. *Nanomedicine* **2018,** *13* (15), 1923-1937.
18. Zepp, R. G.; Hoigne, J.; Bader, H., Nitrate-induced photooxidation of trace organic chemicals in water. *Environ. Sci. Technol.* **1987,** *21* (5), 443-450.
19. Page, S. E.; Logan, J. R.; Cory, R. M.; McNeill, K., Evidence for dissolved organic matter as the primary source and sink of photochemically produced hydroxyl radical in arctic surface waters. *Environ. Sci. Proc. Imp.* **2014,** *16* (4), 807-822.
20. Gligorovski, S.; Strekowski, R.; Barbati, S.; Vione, D., Environmental implications of hydroxyl radicals (•OH). *Chem. Rev.* **2015,** *115* (24), 13051-13092.
21. Miller, P. L.; Chin, Y.-P., Indirect Photolysis Promoted by Natural and Engineered Wetland Water Constituents: Processes Leading to Alachlor Degradation. *Environ. Sci. Technol.* **2005,** *39* (12), 4454-4462.
22. Lam, M. W.; Mabury, S. A., Photodegradation of the pharmaceuticals atorvastatin, carbamazepine, levofloxacin, and sulfamethoxazole in natural waters. *Aquatic Sciences* **2005,** *67* (2), 177-188.
23. Vione, D.; Maddigapu, P. R.; De Laurentiis, E.; Minella, M.; Pazzi, M.; Maurino, V.; Minero, C.; Kouras, S.; Richard, C., Modelling the photochemical fate of ibuprofen in surface waters. *Water Res.* **2011,** *45* (20), 6725-6736.
24. Hou, W.-C.; Henderson, W. M.; Chowdhury, I.; Goodwin, D. G.; Chang, X.; Martin, S.; Fairbrother, D. H.; Bouchard, D.; Zepp, R. G., The contribution of indirect photolysis to the degradation of graphene oxide in sunlight. *Carbon* **2016,** *110*, 426-437.
25. Zepp, R. G.; Faust, B. C.; Hoigne, J., Hydroxyl radical formation in aqueous reactions (pH 3-8) of iron(II) with hydrogen peroxide: the photo-Fenton reaction. *Environ. Sci. Technol.* **1992,** *26* (2), 313-319.
26. Chen, C.-Y.; Jafvert, C. T., Photoreactivity of carboxylated single-walled carbon nanotubes in sunlight: reactive oxygen species production in water. *Environ. Sci. Technol.* **2010,** *44* (17), 6674-6679.
27. Hou, W.-C.; BeigzadehMilani, S.; Jafvert, C. T.; Zepp, R. G., Photoreactivity of unfunctionalized single-wall carbon nanotubes involving hydroxyl radical: chiral dependency and surface coating effect. *Environ. Sci. Technol.* **2014,** *48* (7), 3875-3882.
28. Hou, W.-C.; Chowdhury, I.; Goodwin, D. G.; Henderson, W. M.; Fairbrother, D. H.; Bouchard, D.; Zepp, R. G., Photochemical transformation of graphene oxide in sunlight. *Environ. Sci. Technol.* **2015,** *49* (6), 3435-3443.
29. Hou, W.-C.; Jafvert, C. T., Photochemical transformation of aqueous C60 clusters in sunlight. *Environ. Sci. Technol.* **2009,** *43* (2), 362-367.
30. Sanchís, J.; Aminot, Y.; Abad, E.; Jha, A. N.; Readman, J. W.; Farré, M., Transformation of C60 fullerene aggregates suspended and weathered under realistic environmental conditions. *Carbon* **2018,** *128*, 54-62.
31. Chen, X.; Fang, G.; Liu, C.; Dionysiou, D. D.; Wang, X.; Zhu, C.; Wang, Y.; Gao, J.; Zhou, D., Cotransformation of carbon dots and contaminant under light in aqueous solutions: a mechanistic study. *Environ. Sci. Technol.* **2019,** *53* (11), 6235-6244.
32. de Medeiros, T. V.; Manioudakis, J.; Noun, F.; Macairan, J.-R.; Victoria, F.; Naccache, R., Microwave-assisted synthesis of carbon dots and their applications. *J. Mater. Chem. C* **2019,** *7* (24), 7175-7195.
33. Zhi, B.; Gallagher, M. J.; Frank, B. P.; Lyons, T. Y.; Qiu, T. A.; Da, J.; Mensch, A. C.; Hamers, R. J.; Rosenzweig, Z.; Fairbrother, D. H.; Haynes, C. L., Investigation of phosphorous doping effects on polymeric carbon dots: fluorescence, photostability, and environmental impact. *Carbon* **2018,** *129*, 438-449.
34. Lankone, R. S.; Barclay, M.; Deline, A. R.; Fairbrother, D. H., Quantifying hydroxyl radical concentrations and total dose via principle component analysis of UV-Vis Spectroscopy. *Anal. Methods* **Submitted**.

35. Haag, W. R.; Hoigné, J., Photo-sensitized oxidation in natural water via .OH radicals. *Chemosphere* **1985,** *14* (11), 1659-1671.
36. Schneider, J.; Reckmeier, C. J.; Xiong, Y.; von Seckendorff, M.; Susha, A. S.; Kasák, P.; Rogach, A. L., Molecular fluorescence in citric acid-based carbon dots. *J. Phys. Chem. C* **2017,** *121* (3), 2014-2022.
37. Yuan, H.; Yu, J.; Feng, S.; Gong, Y., Highly photoluminescent pH-independent nitrogen-doped carbon dots for sensitive and selective sensing of p-nitrophenol. *RSC Adv.* **2016,** *6* (18), 15192-15200.
38. Max, J.-J.; Chapados, C., Infrared spectroscopy of aqueous carboxylic acids: malic acid. *J. Phys. Chem. A* **2002,** *106* (27), 6452-6461.
39. Dousseau, F.; Pezolet, M., Determination of the secondary structure content of proteins in aqueous solutions from their amide I and amide II infrared bands. Comparison between classical and partial least-squares methods. *Biochemistry* **1990,** *29* (37), 8771-8779.
40. Liu, W.; Li, C.; Ren, Y.; Sun, X.; Pan, W.; Li, Y.; Wang, J.; Wang, W., Carbon dots: surface engineering and applications. *J. Mater. Chem. B* **2016,** *4* (35), 5772-5788.
41. Colthup, N. B., Spectra-structure correlations in the infra-red region. *J. Opt. Soc. Am.* **1950,** *40* (6), 397-400.
42. Wishart, D. S.; Case, D. A., [1] - Use of Chemical Shifts in Macromolecular Structure Determination. In *Methods in Enzymology*, James, T. L.; Dötsch, V.; Schmitz, U., Eds. Academic Press: 2002; Vol. 338, pp 3-34.
43. Fouda, A. S.; Elmorsi, M. A.; Shaban, S. M.; Fayed, T.; Azazy, O., Evaluation of N-(3-(dimethyl hexadecyl ammonio)propyl) palmitamide bromide as cationic surfactant corrosion inhibitor for API N80 steel in acidic environment. *Egypt. J. Pet.* **2018,** *27* (4), 683-694.
44. Shaban, S. M., N-(3-(Dimethyl benzyl ammonio)propyl)alkanamide chloride derivatives as corrosion inhibitors for mild steel in 1 M HCl solution: experimental and theoretical investigation. *RSC Adv.* **2016,** *6* (46), 39784-39800.
45. Szilágyi, L.; Jardetzky, O., α-Proton chemical shifts and secondary structure in proteins. *Journal of Magnetic Resonance (1969)* **1989,** *83* (3), 441-449.
46. Blundell, C. D.; DeAngelis, P. L.; Day, A. J.; Almond, A., Use of 15N-NMR to resolve molecular details in isotopically-enriched carbohydrates: sequence-specific observations in hyaluronan oligomers up to decasaccharides. *Glycobiology* **2004,** *14* (11), 999-1009.
47. Blundell, Charles D.; Deangelis, Paul L.; Almond, A., Hyaluronan: the absence of amide–carboxylate hydrogen bonds and the chain conformation in aqueous solution are incompatible with stable secondary and tertiary structure models. *Biochem J.* **2006,** *396* (3), 487-498.
48. Hill, S. A.; Benito-Alifonso, D.; Davis, S. A.; Morgan, D. J.; Berry, M.; Galan, M. C., Practical three-minute synthesis of acid-coated fluorescent carbon dots with tuneable core structure. *Sci. Rep.* **2018,** *8* (1), 12234.
49. Stadtman, E. R., Oxidation of free amino acid and amino acid residues in proteins by radiolysis and by metal-catalyzed reactions. *Annu. Rev. Biochem.* **1993,** *62* (1), 797-821.
50. Zhao, P.; Zhu, L., Dispersibility of carbon dots in aqueous and/or organic solvents. *Chemical Communications* **2018,** *54* (43), 5401-5406.
51. Zhang, B.; Liu, C.-y.; Liu, Y., A Novel One-Step Approach to Synthesize Fluorescent Carbon Nanoparticles. *European Journal of Inorganic Chemistry* **2010,** *2010* (28), 4411-4414.
52. Xu, M.; Xu, S.; Yang, Z.; Shu, M.; He, G.; Huang, D.; Zhang, L.; Li, L.; Cui, D.; Zhang, Y., Hydrophilic and blue fluorescent N-doped carbon dots from tartaric acid and various alkylol amines under microwave irradiation. *Nanoscale* **2015,** *7* (38), 15915-15923.
53. Wang, W.; Damm, C.; Walter, J.; Nacken, T. J.; Peukert, W., Photobleaching and stabilization of carbon nanodots produced by solvothermal synthesis. *Physical Chemistry Chemical Physics* **2016,** *18* (1), 466-475.
54. Fiuza, T.; Gomide, G.; Campos, A. F. C.; Messina, F.; Depeyrot, J., On the Colloidal Stability of Nitrogen-Rich Carbon Nanodots Aqueous Dispersions. *C — Journal of Carbon Research* **2019,** *5* (4), 74.

631 55. Smith, B.; Wepasnick, K.; Schrote, K. E.; Cho, H.-H.; Ball, W. P.; Fairbrother, D. H., Influence
632 of Surface Oxides on the Colloidal Stability of Multi-Walled Carbon Nanotubes: A Structure−Property
633 Relationship. *Langmuir* **2009,** *25* (17), 9767-9776.
634 56. Zhang, L.; Wang, M.; Fang, J.; Yang, K.; Lin, D., The effect of oxidation on physicochemical
635 properties and aqueous stabilization of multiwalled carbon nanotubes: comparison of multiple analysis
636 methods. *Science China Chemistry* **2016,** *59* (11), 1498-1507.
637 57. Bai, Y.; Wu, F.; Lin, D.; Xing, B., Aqueous stabilization of carbon nanotubes: effects of surface
638 oxidization and solution chemistry. *Environmental Science and Pollution Research* **2014,** *21* (6), 4358-
639 4365.
640 58. Hadadian, M.; Goharshadi, E. K.; Youssefi, A., Electrical conductivity, thermal conductivity, and
641 rheological properties of graphene oxide-based nanofluids. *Journal of Nanoparticle Research* **2014,** *16*
642 (12), 2788.
643 59. Nuncira, J.; Seara, L. M.; Sinisterra, R. D.; Caliman, V.; Silva, G. G., Long-term colloidal
644 stability of graphene oxide aqueous nanofluids. *Fullerenes, Nanotubes and Carbon Nanostructures* **2019**,
645 1-11.
646 60. Qi, Y.; Xia, T.; Li, Y.; Duan, L.; Chen, W., Colloidal stability of reduced graphene oxide
647 materials prepared using different reducing agents. *Environ. Sci.: Nano* **2016,** *3* (5), 1062-1071.
648 61. Iogansen, A. V.; Litovchenko, G. D., The characteristic bands of the stretching vibrations of the
649 nitro group in infrared absorption. *J. Appl. Spectrosc.* **1965,** *3* (6), 404-411.
650 62. Barańska, H.; Kuduk-Jaworska, J.; Szostak, R.; Romaniewska, A., Vibrational spectra of racemic
651 and enantiomeric malic acids. *J. Raman Spectrosc.* **2003,** *34* (1), 68-76.
652 63. Brooker, M. H.; Irish, D. E., Vibrational frequency assignments of isotopically different forms of
653 nitrate ion in ionic nitrate crystals. *Can. J. Chem.* **1970,** *48* (8), 1198-1201.
654 64. Howarth, O. W.; Lilley, D. M. J., Carbon-13-NMR of peptides and proteins. *Prog. Nucl. Mag.*
655 *Res. Sp.* **1978,** *12* (1), 1-40.
656 65. Katsuraya, K.; Hatanaka, K.; Matsuzaki, K.; Amiya, S., Assignment of finely resolved 13C NMR
657 spectra of poly(vinyl alcohol). *Polymer* **2001,** *42* (24), 9855-9858.
658 66. Ding, S.; Hong, Y.-W.; Chen, C.-Y.; Chang, N.-C., One and two dimensional 1H and 13C high
659 resolution NMR investigation of lariat ethers and their alkali metal ionic complexes: A more tangible
660 evidence for the presence of less common C–H···O hydrogen bonds. *Biophys. Chem.* **2006,** *121* (2), 75-
661 83.
662 67. Gilbert, A.; Yamada, K.; Yoshida, N., Exploration of intramolecular 13C isotope distribution in
663 long chain n-alkanes (C11–C31) using isotopic 13C NMR. *Org. Geochem.* **2013,** *62*, 56-61.
664 68. Ritter, W.; Hull, W.; Cantow, H. J., Determination of the most stable conformers of branched
665 alkanes by 13C-NMR spectroscopy at very low temperatures. *Tetrahedron Lett.* **1978,** *19* (34), 3093-
666 3096.
667 69. Doan, H. Q.; Davis, A. C.; Francisco, J. S., Primary steps in the reaction of OH radicals with
668 peptide systems: perspective from a study of model amides. *J. Phys. Chem. A* **2010,** *114* (16), 5342-5357.
669 70. Vel Leitner, N. K.; Berger, P.; Legube, B., Oxidation of amino groups by hydroxyl radicals in
670 relation to the oxidation degree of the α-carbon. *Environ. Sci. Technol.* **2002,** *36* (14), 3083-3089.
671 71. Quici, N.; Morgada, M. E.; Gettar, R. T.; Bolte, M.; Litter, M. I., Photocatalytic degradation of
672 citric acid under different conditions: TiO2 heterogeneous photocatalysis against homogeneous photolytic
673 processes promoted by Fe(III) and H2O2. *Appl. Catal. B-Environ.* **2007,** *71* (3), 117-124.
674 72. Pelizzetti, E.; Minero, C.; Piccinini, P.; Vincenti, M., Phototransformations of nitrogen containing
675 organic compounds over irradiated semiconductor metal oxides: Nitrobenzene and Atrazine over TiO2
676 and ZnO. *Coordin. Chem. Rev.* **1993,** *125* (1), 183-193.
677 73. Hwang, Y. S.; Li, Q., Characterizing photochemical transformation of aqueous nC60 under
678 environmentally relevant conditions. *Environ. Sci. Technol.* **2010,** *44* (8), 3008-3013.
679
680

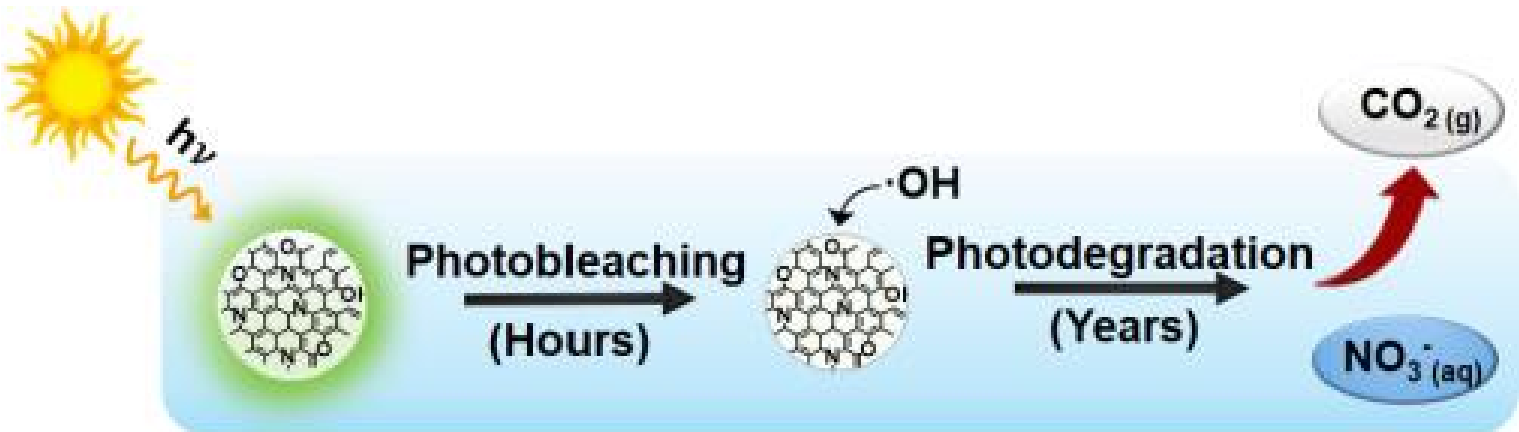

ACS Paragon Plus Environment